In Search for Mononuclear Helical Lanthanide Building Blocks with Predetermined Properties: Lanthanide Complexes with Diethyl Pyridine-2,6-dicarboxylate

Fabien Renaud, Claude Piguet,* Gérald Bernardinelli, Jean-Claude G. Bünzli,* and Gérard Hopfgartner

Abstract: The ligand diethyl pyridine-2,6-dicarboxylate ($\mathbf{L^5}$) reacts with Ln^{III} in acetonitrile to successively give the complexes $[Ln(\mathbf{L^5})_i]^{3+}$ (Ln = La to Lu, $i = 1-3$). Spectroscopic investigations (ES-MS, UV/Vis, NMR) show that the 1:3 complexes $[Ln(\mathbf{L^5})_3]^{3+}$ have poor stability in solution and exist as a mixture of rapidly interconverting conformers. Variable-temperature NMR data show that the helical $P \rightleftharpoons M$ interconversion and dynamic on–off equilibria of the ester side arms both control the observed average structure in solution. Contrary to similar lanthanide building blocks possessing benzimidazole or carboxamide side arms, $[Eu(\mathbf{L^5})_3]^{3+}$ has a sizable quantum yield in anhydrous acetonitrile; this has been attributed to an improved ligand → Eu^{III} energy transfer resulting from a good energetic match between the ligand- and metal-centered excited states. Pure 1:3 complexes cannot be isolated in the solid state, but crystalline 1:2 complexes $[Ln(\mathbf{L^5})_2](TfO)_3 \cdot nH_2O$ have been prepared. The X-ray crystal structure of $[Eu(\mathbf{L^5})_2(TfO)_2(OH_2)]TfO$ (**1**) reveals two meridionally tricoordinated ligands $\mathbf{L^5}$, but the long Eu–O(ester) bonds imply only weak interactions between the carbonyl groups of the ester side arms and Eu^{III}, providing a limited protection of the metallic site. The photophysical studies show that nonacoordinate Eu^{III} in **1** binds an additional water molecule to give a decacoordinate complex in the solid state, thus confirming the accessibility of the metallic site for further complexation.

Keywords
esters · helical structures · lanthanides · luminescence · tridentate ligands

Introduction

The wrapping of meridionally tricoordinated ligand strands around trivalent lanthanide ions (Ln^{III}) produces well-protected coordination sites with structural and electronic characteristics that can be finely tuned by secondary weak noncovalent interactions.[1] Interstrand π-stacking between benzimidazole side arms in $[Ln(\mathbf{L^1})_3]^{3+}$ are responsible for the significant size-discriminating effects[2] and luminescence quenching,[3] steric constraints in $[Ln(\mathbf{L^2})_3]^{3+}$ affect the dynamic and structural properties in solution,[4] and electrostatic effects in $[Ln(\mathbf{L^3})_3]^{3-}$ induce structural variations along the Ln^{III} series (see Scheme 1 for ligand structures).[5] Systematic investigations of $\mathbf{L^1}$[2, 3, 6] and $\mathbf{L^2}$[4] lead to the conclusion that a combination of benzimidazole and carboxamide side arms bound to the 2,6-positions of the central pyridine ring are suitable for the design of triple-helical lanthanide building blocks with predetermined properties, as exemplified by the recent preparation of functional noncovalent lanthanide podates $[LnM(\mathbf{L^4})_3]^{5+}$ (M = Zn,[7] M = Fe[8]).

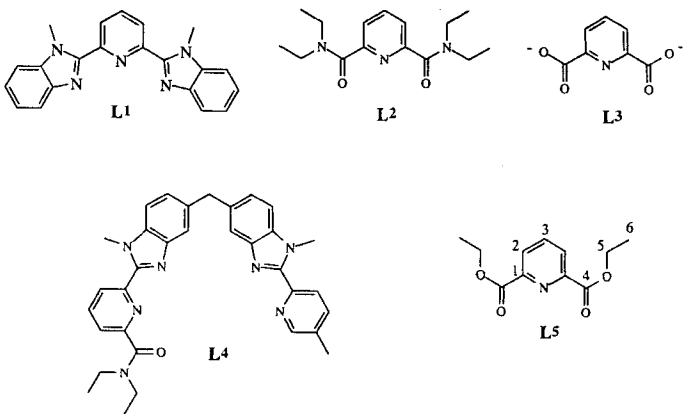

Scheme 1.

[*] C. Piguet, F. Renaud
Department of Inorganic, Analytical and Applied Chemistry
University of Geneva, 30 quai E. Ansermet, 1211 Geneva 4 (Switzerland)
Fax: Int. code +(4122) 702-6069
e-mail: claude.piguet@chiam.unige.ch
G. Bernardinelli
Laboratory of X-ray Crystallography
24 quai E. Ansermet, 1211 Geneva 4 (Switzerland)
J.-C. G. Bünzli
Institute of Inorganic and Analytical Chemistry
University of Lausanne, BCH 1402, 1015 Lausanne (Switzerland)
G. Hopfgartner
F. Hoffmann-La Roche, Pharmaceuticals Division
Department of Drug Metabolism and Kinetics, 4070 Basle (Switzerland)

0947-6539/97/0310-1660 $ 17.50+.50/0

The investigation of ligand $\mathbf{L^5}$ with ester side arms is thus a logical development to broaden the scope of these new programmed lanthanide building blocks.

Although systematically used as protecting groups during the syntheses of receptors with pendant carboxylate arms,[9] ester groups have not stirred much interest as coordinating moieties for Ln^{III} ions,[10] probably as a result of the low electronic density on the oxygen atom of the carbonyl function compared to that found in carboxylates and carboxamides.[11] Recent attempts to introduce 2,6-pyridinedicarboxylic functionalities analogous to $\mathbf{L^5}$ into a macrocyclic bislactone for the complexation of Ln^{III} failed.[12] However, an acyclic derivative with dangling ether and ester side arms has been shown to produce stable and luminescent complexes with Eu^{III} and Tb^{III}, although it is not clear whether or not the ester groups are bound in the inner coordination sphere.[12]

In this paper, we report the formation of lanthanide complexes $[Ln(\mathbf{L^5})_i]^{3+}$ $(i = 1-3)$ where the versatile ester side arms interact with Ln^{III}. Particular attention has been focused on the solution behavior and its relevance to the solid-state structures.

Results and Discussions

Complexes of $\mathbf{L^5}$ with Ln^{III} in solution: The ES-MS titration of $\mathbf{L^5}$ (total concentration 2×10^{-4} M) in acetonitrile with $La(TfO)_3\cdot3H_2O$ for the ratio $\mathbf{L^5}$:La^{III} in the range of 1–4 reveals the presence of intricate mixtures of the successive complexes $[La(\mathbf{L^5})_i]^{3+}$ $(i = 2-6)$ together with their adducts with trifluoromethanesulfonate (TfO) anions $[La(\mathbf{L^5})_i(TfO)_j]^{(3-j)+}$ $(j = 1, 2$; Table 1). Peaks assigned to the free ligand (m/z = 224.0 $[\mathbf{L^5}+H]^+$ and m/z = 447.0 $[2\,\mathbf{L^5}+H]^+$) are observed during the titration, but a quantitative interpretation is precluded by the variable responses of Ln^{III} complexes to ES-MS.[4, 13] Nevertheless, general trends emerge from the ES-MS data:

Table 1. Molecular peaks of complexes and adduct ions observed for the ES-MS titration of $\mathbf{L^5}$ with $La(TfO)_3\cdot3H_2O$ in acetonitrile [a].

Metal	Cation	m/z [a]	Metal	Cation	m/z [a]
La^{III}	$[\mathbf{L^5}+H]^+$	224.0	La^{III}	$[La(\mathbf{L^5})_3(TfO)_2]^+$	1106.2
	$[(\mathbf{L^5})_2+H]^+$	447.0		$[La(\mathbf{L^5})_4]^{3+}$	343.8
	$[La(\mathbf{L^5})_2]^{3+}$	194.6		$[La(\mathbf{L^5})_4(TfO)]^{2+}$	590.2
	$[La(\mathbf{L^5})_2(TfO)]^{2+}$	367.2		$[La(\mathbf{L^5})_5]^{3+}$	418.2
	$[La(\mathbf{L^5})_2(TfO)_2]^+$	883.0		$[La(\mathbf{L^5})_5(TfO)]^{2+}$	701.6
	$[La(\mathbf{L^5})_3]^{3+}$	269.4		$[La(\mathbf{L^5})_6]^{3+}$	492.5
	$[La(\mathbf{L^5})_3(TfO)]^{2+}$	478.6		$[La(\mathbf{L^5})_6(TfO)]^{2+}$	813.2

[a] m/z values given for the maximum of the peak.

1) The 1:1 complex $[La(\mathbf{L^5})]^{3+}$ is not observed, in agreement with its expected large solvation energy, associated with a faint ES-MS response,[4, 14] and its limited stability.
2) $[La(\mathbf{L^5})_i]^{3+}$ ions $(i = 2-6)$ are detected during the entire titration, but the variable intensities of the peaks corresponding to the species $[La(\mathbf{L^5})_i(TfO)_j]^{(3-j)+}$ $(j = 0-2)$ for a given i value and at different La:$\mathbf{L^5}$ ratios preclude any semiquantitative analyses.
3) The substoichiometric complexes $[La(\mathbf{L^5})_i]^{3+}$ $(i = 4-6)$ give intense ES-MS signals, while only negligible peaks are observed for $[Ln(\mathbf{L^2})_4]^{3+}$ under the same conditions.[4]

The origin of these substoichiometric complexes $[La(\mathbf{L^5})_i]^{3+}$ $(i = 4-6)$ is not clear, and we cannot infer from the ES-MS spectra whether they reflect solution or gas-phase behavior, but we notice that the adducts with two anions $[La(\mathbf{L^5})_i(TfO)_2]^+$ $(i = 4-6)$ are systematically missing in the spectra (Table 1); this strongly suggests a reduced charge density on the complexes $[La(\mathbf{L^5})_i]^{3+}$, in agreement with their expected larger size.[15]

According to our experience of the ES-MS spectra of Ln^{III} complexes,[13] we suspect that the observation of substoichiometric complexes indeed reflects the accessibility of the charged metallic center for further complexation. This effect is not observed for $[Ln(\mathbf{L^1})_3]^{3+}$, since the metal ion is efficiently shielded from external interaction by the three wrapped aromatic strands.[16] In contrast, traces of $[Ln(\mathbf{L^2})_4]^{3+}$ are observed by ES-MS for Ln = La–Nd; here, the structures of the precursor triple-helical complexes $[Ln(\mathbf{L^2})_3]^{3+}$ are less relaxed in solution.[4] The fact that this behavior becomes dominant for $\mathbf{L^5}$ indicates that the metal ion is more accessible for further complexation.

The UV spectrum of $\mathbf{L^5}$ is characterized by overlapping broad bands assigned to $n \rightarrow \pi^*$ and $\pi \rightarrow \pi^*$ transitions,[2] which are sufficiently affected by complexation to allow the spectrophotometric monitoring of the titrations of $\mathbf{L^5}$ $(10^{-3}$ M) with $Ln(TfO)_3\cdot nH_2O$ (Ln = La, Pr, Sm, Tb, Tm, Lu, Y) for Ln:$\mathbf{L^5}$ ratios in the range of 0.1–2.0 (Table 2). The collected data show a smooth and continuous variation of the molar extinction with a single end point for Ln:$\mathbf{L^5}$ = 1, in contrast with the pronounced inflection observed previously for Ln:$\mathbf{L^2}$ = 0.33 under the same conditions.[4] This implies a lower stability for $[Ln(\mathbf{L^5})_3]^{3+}$ compared to $[Ln(\mathbf{L^2})_3]^{3+}$. Factor analyses[17] are compatible with the existence of four absorbing species $\mathbf{L^5}$ and $[Ln(\mathbf{L^5})_i]^{3+}$ $(i = 1-3)$, and the data can be satisfactorily fitted to this model yielding stability constants reported in Table 3.

Table 2. Ligand-centered absorptions for $\mathbf{L^5}$ and its complexes $[Ln(\mathbf{L^5})_3]^{3+}$ (Ln = Eu, Tb) in acetonitrile solution at 293 K [a].

Compd	Absorption ($\pi \rightarrow \pi^* + n \rightarrow \pi^*$)
$\mathbf{L^5}$	45250 (8420); 38020 (3370, sh); 37040 (3490); 36100 (2520, sh)
$[Eu(\mathbf{L^5})_3]^{3+}$	47170 (27580); 44050 (20250, sh); 37450 (8850, sh); 36500 (12200); 35460 (11120, sh)
$[Tb(\mathbf{L^5})_3]^{3+}$	47170 (27090); 44050 (20730, sh); 37450 (9300, sh); 36500 (12720); 35460 (11350, sh)

[a] Energies are given for the maximum of the band envelope in cm^{-1}, and the molar absorption coefficient (ε) is given in parentheses in $M^{-1}cm^{-1}$. Sh: shoulder.

Table 3. Cumulative stability constants ($\log(\beta_i^{1:n})$) for $[Ln(\mathbf{L^5})_i]^{3+}$ $(i = 1-3)$ in acetonitrile at 293 K.

Metal	$\log(\beta_1)$	$\log(\beta_2)$	$\log(\beta_3)$
La^{III}	6.8(3)	12.8(4)	16.3(4)
Pr^{III}	6.9(4)	13.0(4)	16.6(4)
Sm^{III}	6.9(4)	13.3(4)	17.0(4)
Tb^{III}	6.9(4)	13.5(4)	17.3(4)
Y^{III}	6.9(4)	13.5(4)	17.3(4)
Tm^{III}	7.0(4)	13.7(4)	17.6(4)
Lu^{III}	7.0(4)	14.0(4)	18.0(4)

  0947-6539/97/0310-1661 $ 17.50+.50/0

Table 4. NMR shifts (with respect to TMS) for ligand $\mathbf{L^5}$ and its complexes $[Ln(\mathbf{L^5})_3]^{3+}$ in CD_3CN at 298 K [a].

Compd	H^2	H^3	$H^{5,5'}$	H^6	C^1	C^2	C^3	C^4	C^5	C^6
$\mathbf{L^5}$	8.30	8.01	4.50	1.47	148.48	127.70	138.13	164.49	62.20	14.09
$[La(\mathbf{L^5})_3]^{3+}$	8.37	8.34	4.55	1.42	147.47	129.78	142.64	168.84	65.76	14.16
$[Y(\mathbf{L^5})_3]^{3+}$	8.42	8.42	4.49	1.37	146.79	130.04	143.81	169.63	66.77	13.99
$[Lu(\mathbf{L^5})_3]^{3+}$	8.49	8.55	4.43	1.32	145.96	130.83	145.50	172.17	68.46	13.81
$[Ce(\mathbf{L^5})_3]^{3+}$	11.25	10.88	2.50	0.33	159.74	137.03	146.50	172.18	64.74	12.95
$[Pr(\mathbf{L^5})_3]^{3+}$	11.03	10.53	3.05	0.69	157.43	143.21	144.20	176.53	65.77	13.14
$[Nd(\mathbf{L^5})_3]^{3+}$	12.89	12.31	0.78	−0.53	165.48	144.60	147.50	174.83	63.64	11.94
$[Sm(\mathbf{L^5})_3]^{3+}$	8.64	8.64	4.16	1.22	149.61	129.98	143.73	169.96	65.75	13.87
$[Eu(\mathbf{L^5})_3]^{3+}$	5.64	6.42	6.71	2.37	139.81	104.90	149.24	181.50	66.89	15.54

[a] See Scheme 1 for numbering.

Although, the differences between the calculated UV spectra of the absorbing species are significant, attempts to introduce supplementary equilibria involving substoichiometric complexes $[Ln(\mathbf{L^5})_i]^{3+}$ ($i = 4-6$) failed. The stability constants $\log(\beta_1^{Ln})$ and $\log(\beta_2^{Ln})$ of $[Ln(\mathbf{L^5})_i]^{3+}$ are smaller by approximately one order of magnitude than those found for the carboxamide analogues $[Ln(\mathbf{L^2})_i]^{3+}$.[4] The comparison of $\log(\beta_3^{Ln})$ is more striking, since $[Ln(\mathbf{L^5})_3]^{3+}$ ions are less stable than $[Ln(\mathbf{L^2})_3]^{3+}$ ions by a factor 10^4-10^5 in acetonitrile. This dramatic effect is attributed to the weaker interactions between Ln^{III} and the ester groups of $\mathbf{L^5}$, which are in competition with the poorly coordinating triflate anions for the coordination of the third tridentate ligand.[18] As found for $[Ln(\mathbf{L^2})_i]^{3+}$,[4] $\log(\beta_i^{Ln})$ ($i = 1-3$) increase smoothly with decreasing ionic radii (R^j)[19] leading to straight lines for plots of $\log(\beta_1^{Ln})$ vs. $1/R^j$, typical of electrostatic interactions (Figure 1).[4] According to statistical factors and steric hindrance,[20] the successive stability constants $\log(K_i^{Ln})$ ($i \geq 4$) for the formation of possible substoichiometric complexes in solution are expected to be significantly lower than $\log(K_3^{Ln}) \approx 3.5-4.0$ and thus difficult to address under our experimental conditions.

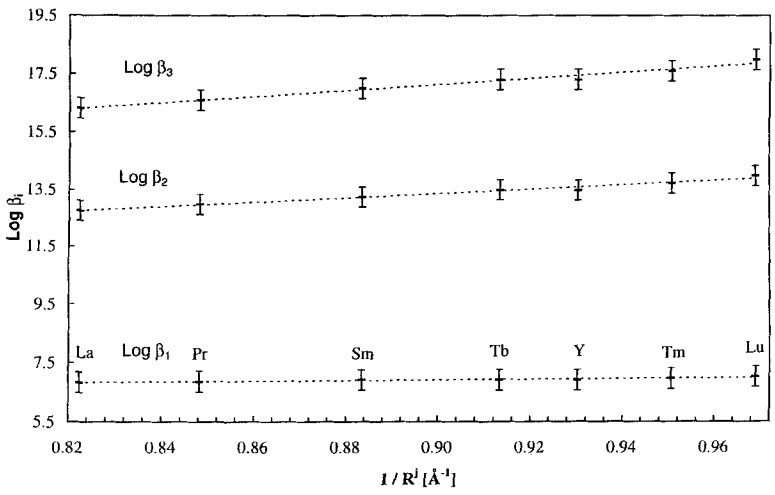

Figure 1. Stability constants $\log(\beta_i^{Ln})$ for $[Ln(\mathbf{L^5})_i]^{3+}$ ($i = 1-3$) vs. $1/R^j$ (R^j ionic radii of nonacoordinate Ln^{III}) [19].

The ^1H and ^{13}C NMR spectra in CD_3CN are recorded for $Ln:\mathbf{L^5} = 0.33$ and a total ligand concentration of 0.1 M, which ensures the almost quantitative formation (>92%) of $[Ln(\mathbf{L^5})_3]^{3+}$ in solution. The $^{13}C\{^1H\}$ NMR spectra of the diamagnetic complexes $[Ln(\mathbf{L^5})_3]^{3+}$ (Ln = La, Y, Lu) display six signals attributed to C^{1-6}, according to 2D heteronuclear $\{^{13}C-^1H\}$ correlation spectroscopy. This pattern corresponds to D_3 or D_{3h} symmetries for the complexes on the NMR timescale (Table 4). Compared to those of the free ligand $\mathbf{L^5}$, the signals of C^2 ($\Delta\delta = +2.18$), C^3 ($\Delta\delta = +4.51$), and C^4 ($\Delta\delta = +4.35$) in $[La(\mathbf{L^5})_3]^{3+}$ are significantly deshielded, implying the simultaneous N-coordination of the pyridine ring[22] and O-coordination of the carbonyl group to La^{III},[23] as similarly found for $[La(\mathbf{L^2})_3]^{3+}$.[4] The downfield shifts increase with smaller Ln^{III} ions, reaching a maximum for $[Lu(\mathbf{L^5})_3]^{3+}$ (C^2: $\Delta\delta = +3.13$, C^3: $\Delta\delta = +7.37$, C^4: $\Delta\delta = +7.68$) and pointing to an improved drainage of the electron density onto the smaller Ln^{III} ions (Table 4). The ^1H NMR spectra of $[Ln(\mathbf{L^5})_3]^{3+}$ (Ln = La, Y) display only one resolved quartet assigned to the methylene protons $H^{5,5'}$ and compatible with an average D_{3h} symmetry at 298 K, as previously discussed for $[La(\mathbf{L^2})_3]^{3+}$ under the same conditions.[4] For $[Lu(\mathbf{L^5})_3]^{3+}$, a broad multiplet is observed at 298 K, which is resolved into a quartet at 333 K associated with the average D_{3h} symmetry on the NMR timescale. Fast interconversion processes between the $P \rightleftharpoons M$ enantiomers of the triple-helical complex may account for the observed behavior at high temperature, and we thus expect that the broad multiplet observed at 298 K should give two sextuplets (ABX_3 spin system) at low temperature, as observed for $[Lu(\mathbf{L^2})_3]^{3+}$.[4] Variable-temperature ^1H NMR spectra of $[Lu(\mathbf{L^5})_3]^{3+}$ indeed show the appearance of second-order multiplets at 243 K, which can be assigned to two sets of two "sextuplets" with respective intensities of 2:2:1:1 at 233 K (Figure 2). This observation can be only rationalized with the simultaneous consideration of dynamic $P \rightleftharpoons M$ helical interconversion together with on–off coordination of the ester side arms, as previously invoked for distal pyridine side arms in $[Eu(terpy)_3]^{3+}$ (terpy = 2,2′:6′,2″-terpyridine) dissolved in acetonitrile.[24] Addition of an excess of $\mathbf{L^5}$ to the solution produces new signals corresponding to the free ligand (slow exchange regime), which partially overlap the two sextuplets at high field ($\delta = 4.22$, Figure 2); this strongly suggests that the latter signals correspond to decomplexed ester side arms, while the two sextuplets at lower field ($\delta = 4.40$, Figure 2) are assigned to coordinated ester groups. The consideration of the relative integrated intensities of the four sextuplets leads to the conclusion that $[Lu(\mathbf{L^5})_3]^{3+}$ possesses roughly 33% uncomplexed ester side arms leading to an

0947-6539/97/0310-1662 $ 17.50+.50/0 Chem. Eur. J. 1997, 3, No. 10

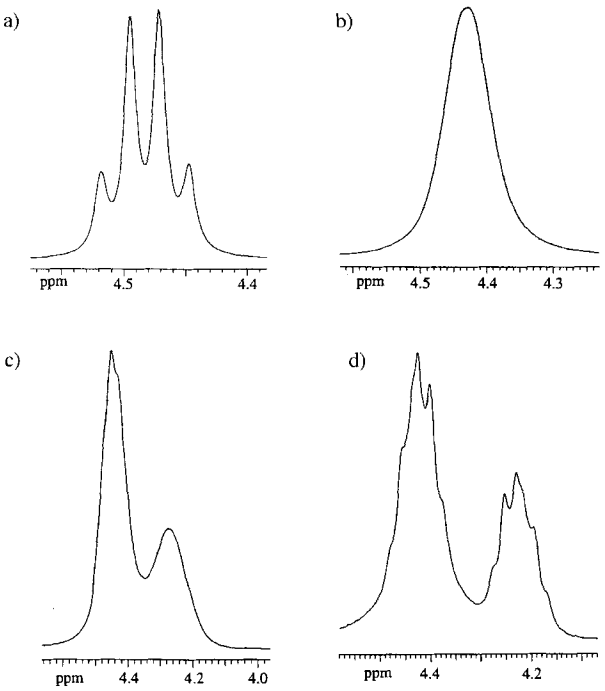

Figure 2. Part of the ^{1}H NMR spectra of $[Lu(\mathbf{L^5})_3]^{3+}$ in CD_3CN showing the signals of the methylene protons $H^{5,5'}$ at a) 333 K, b) 298 K, c) 253 K, and d) 233 K.

average coordination of four ester groups on the ^{1}H NMR timescale at 233 K. This semiquantitative analysis is corroborated by the splitting of the signal assigned to the methyl C^6 protons into two triplets in a 1:2 ratio at 233 K. The pyridine protons are broadened at low temperature, but do not show splitting patterns or significant upfield shifts at 233 K associated with decomplexation of the pyridine ring. We conclude that the N-coordination of the central pyridine ring is maintained on average, as previously reported for similar on–off equilibria in $[Eu(terpy)_3]^{3+}$.[24] This behavior contrasts with that observed for $[Lu(\mathbf{L^2})_3]^{3+}$ where only $P \rightleftharpoons M$ helical interconversions have been demonstrated,[4] pointing to the lower affinity of ester side arms in $\mathbf{L^5}$ for Ln^{III} compared to carboxamide groups in $\mathbf{L^2}$, a result in line with our thermodynamic data.

It is expected that both contact and pseudo-contact contributions to the induced lanthanide isotropic paramagnetic shift (δ_{ij}^{iso}) will be affected by geometrical and structural changes associated with isomerization and decomplexation processes of the ligand in $[Ln(\mathbf{L^5})_3]^{3+}$ (Ln is a paramagnetic lanthanide).[25] A straightforward separation of contact and pseudo-contact contributions as described for $[Ln(\mathbf{L^2})_3]^{3+}$ [4] requires an isostructural series of complexes. This condition is not met with $\mathbf{L^5}$, the NMR shifts at a given temperature reflecting a slightly different average structure for each Ln^{III}. The NMR spectra of the paramagnetic series $[Ln(\mathbf{L^2})_3]^{3+}$ (Ln = Ce, Pr, Nd, Sm, Eu) at 298 K are compatible with the average D_{3h} symmetry found for Ln = La, Y, but diagnostic criteria of isostructurality[4, 25] clearly show that no satisfying linear correlation exists for plots of $\delta_{ij}^{iso}/\langle S_z\rangle_j$ vs. $C_j/\langle S_z\rangle_j$ and δ_{ij}^{iso}/C_j vs. $\langle S_z\rangle_j/C_j$; this precludes further structural investigations based on contact and dipolar contributions (Figure F1 in the Supporting Information).

Isolation of the complexes, and crystal and molecular structures of $[Eu(\mathbf{L^5})_2(TfO)_2(OH_2)]TfO$ (1): Attempts to isolate pure 1:3 complexes $[Ln(\mathbf{L^5})_3](X)_3$ ($X = TfO^-, ClO_4^-$) under various experimental conditions failed for $\mathbf{L^5}$:Ln = 3–6. Elemental analyses revealed the presence of mixtures of 1:2 and 1:3 complexes, as previously observed for other mononuclear triple-helical complexes of low stability, $[Lu(\mathbf{L^1})_3](ClO_4)_3$[6] and $[Lu(terpy)_3](ClO_4)_3$.[26] However, pure 1:2 complexes can be prepared with elemental analyses corresponding to $[Ln(\mathbf{L^5})_2](TfO)_3 \cdot n H_2O$ (**1**: Ln = Eu, $n = 1$; **2**: Ln = Gd, $n = 2$; **3**: Ln = Tb, $n = 1$). The IR spectra in KBr show the expected shift of $\tilde{\nu}$(C=O) toward lower energy (1685 cm^{-1} in **1–3** compared to 1740 cm^{-1} in $\mathbf{L^5}$), which is typical for the coordination of carbonyl group to Ln^{III}.[23] Related shifts of the vibrations associated with the pyridine ring[6] confirm the meridional tricoordination of $\mathbf{L^5}$ in **1–3**, while a split band in the region of $\tilde{\nu}$(OH) indicates water molecules coordinated to Ln^{III}. The complicated pattern observed for triflate vibrations does not allow a clear distinction to be made between coordinated and free TfO^-,[27] but it strongly suggests that both types of anions exist in the complexes **1–3**.

The crystal structure of **1** confirms the IR results and shows a cation $[Eu(\mathbf{L^5})_2(TfO)_2(H_2O)]^+$, where Eu^{III} is nonacoordinated in a low symmetry site by two meridionally tridentate ligands $\mathbf{L^5}$, two monodentate triflate anions, and one water molecule (Figures 3, 4 and Table 5). The coordinated tridentate binding

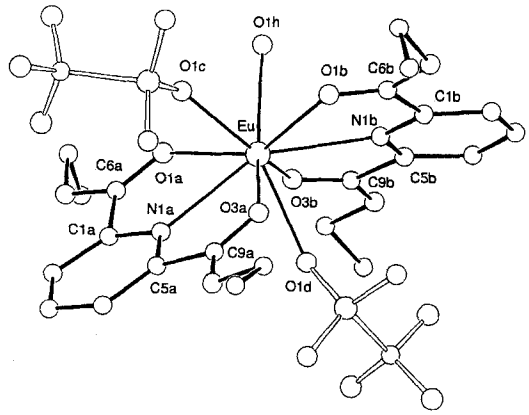

Figure 3. Atomic numbering scheme for $[Eu(\mathbf{L^5})_2(TfO)_2(OH_2)]^+$ (**1**).

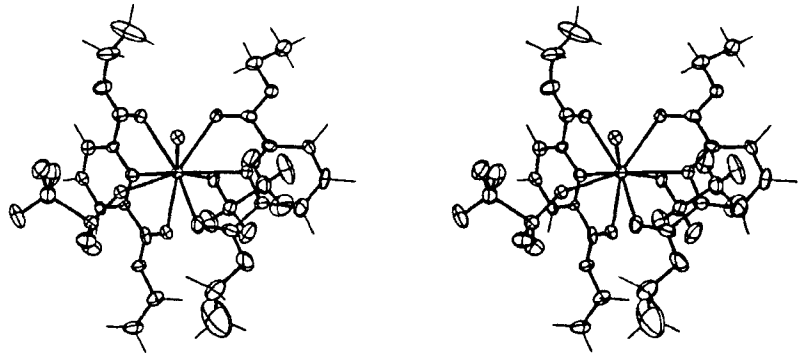

Figure 4. ORTEP [40] stereoview of $[Eu(\mathbf{L^5})_2(TfO)_2(OH_2)]^+$ (**1**) approximately along the Eu–O1h direction.

Table 5. Selected structural data for complex $[Eu(L^5)_2(TfO)_2(OH_2)]TfO$ (**1**).

a) Bond lengths (Å).

Eu-O1a	2.497(7)	Eu-O1b	2.458(7)	Eu-O1c	2.361(6)
Eu-N1a	2.542(8)	Eu-N1b	2.573(7)	Eu-O1d	2.412(8)
Eu-O3a	2.461(7)	Eu-O3b	2.561(6)	Eu-O1h	2.392(8)

b) Bite angles and angles N-Eu-N, O-Eu-N, and O-Eu-O (°).

O1a-Eu-N1a	63.0(3)	O1b-Eu-N1b	63.2(2)
N1a-Eu-O3a	62.9(2)	N1b-Eu-O3b	61.9(2)
O1a-Eu-O3a	125.4(2)	O1b-Eu-O3b	124.1(2)
N1a-Eu-N1b	149.8(3)		
O1a-Eu-N1b	124.0(2)	O1b-Eu-N1a	128.0(2)
O3a-Eu-N1b	106.7(2)	O3b-Eu-N1a	105.0(2)
O1c-Eu-N1b	133.4(3)	O1c-Eu-N1a	74.3(3)
O1d-Eu-N1b	73.0(3)	O1d-Eu-N1a	76.8(3)
O1h-Eu-N1b	75.0(3)	O1h-Eu-N1a	131.0(3)
O1a-Eu-O1b	149.8(3)	O1b-Eu-O1c	76.0(2)
O1a-Eu-O3b	66.0(2)	O1b-Eu-O1d	105.9(3)
O1a-Eu-O1c	82.0(2)	O1b-Eu-O1h	80.7(3)
O1a-Eu-O1d	104.2(3)	O3b-Eu-O1c	142.7(3)
O1a-Eu-O1h	74.3(2)	O3b-Eu-O1d	66.9(3)
O3a-Eu-O1b	69.3(3)	O3b-Eu-O1h	76.3(2)
O3a-Eu-O3b	137.3(3)	O1c-Eu-O1d	143.4(2)
O3a-Eu-O1c	76.7(2)	O1c-Eu-O1h	77.1(2)
O3a-Eu-O1d	70.4(2)	O1d-Eu-O1h	139.4(2)
O3a-Eu-O1h	144.0(2)		

units are almost planar (dihedral angles N1-C5-C9-O4 and N1-C8-C6-O1 in the range -3 to $+5°$) as a result of reduced steric hindrance in 1:2 complexes compared to the bent conformations found for analogous tridentate units in 1:3 complexes $[Eu(L^2)_3]^{3+}$[4] and $[Eu(L^3)_3]^{3-}$.[5] The Eu-O(water) (2.39 Å), Eu-O(triflate) (2.36–2.41 Å), and Eu-N (2.54–2.57 Å) bond lengths are standard,[4, 7, 28] while the Eu-O(ester) bonds (2.46–2.56 Å, average 2.49 Å) are longer than those found for Eu-O(amide) in $[Eu(L^2)_3]^{3+}$ (2.39–2.43 Å)[4] and Eu-O(carboxylate) in $[Eu(L^3)_3]^{3-}$ (2.43–2.45 Å).[5] These differences indicate that the carbonyl O atom of the ester group has a weak affinity for Eu^{III}. The calculated ionic radius of Eu^{III} in **1**, according to Shannon's definition[19] with $r(N) = 1.46$ Å and $r(O) = 1.31$ Å, amounts to 1.13 Å, a value close to the expected radius for nonacoordinate Eu^{III} (1.12 Å).[2, 6, 19]

Photophysical properties of $[Ln(L^5)_2(TfO)_2(OH_2)]TfO$ (1–3) in the solid state: Excitation in the UV absorption bands ($\pi \rightarrow \pi^*$ and $n \rightarrow \pi^*$, Table 2) of the free ligand L^5 produces only faint luminescence (77 K); this points to the efficient nonradiative deactivation pathways in L^5, as reported for L^2.[4] On the other hand, irradiation at 40000 cm^{-1} of the Gd^{III} complex **2** produces a weak, but significant broad emission band (77 K) with a maximum at 32000 cm^{-1} and a long tail at lower energy arising from the $^1\pi\pi^*$ state. This assignment is confirmed by the disappearance of this band in the time-resolved emission spectrum (delay time 0.75 ms) recorded under the same conditions, which reveals one weak structured band centered at 23260 cm^{-1}, attributed to the $^3\pi\pi^*$ excited state.[2–4, 6] Compared to those in $[Gd(L^2)_3](TfO)_3$,[4] the $^1\pi\pi^*$ and $^3\pi\pi^*$ levels in **2** are significantly blue-shifted by 8500 and 2660 cm^{-1}, respectively. Efficient $L^5 \rightarrow Ln^{III}$ energy transfers occur in $[Ln(L^5)_2(TfO)_2(OH_2)]TfO$ (**1**: Ln = Eu; **3**: Ln = Tb) leading to strong metal-centered luminescence at 10, 77, and 295 K. Contrary to $[Ln(L^2)_3](TfO)_3$, **1** and **3** display well-resolved excitation bands in the UV at 77 K (34450–45450 cm^{-1}) assigned to ligand-centered excited states, thus demonstrating that coordinated L^5 is a better sensitizer for Eu^{III} and Tb^{III} than L^2.

A detailed analysis of the Eu^{III} coordination site in **1** can be addressed with high-resolution laser-excited luminescence spectroscopy. Fragile crystals of **1** are separated from the mother liquor, flushed with N_2 and introduced into the cryostat. The excitation spectrum at 10 K (Figure 5) displays two well-resolved $^5D_0 \leftarrow {}^7F_0$ transitions at 17268 cm^{-1} (full width at half height (fwhh) = 1.19 cm^{-1}) and 17277 cm^{-1} (fwhh = 1.49 cm^{-1}) corresponding to two different Eu^{III} environments labeled sites I and II, respectively. Selective laser excitations yield $^5D_0 \rightarrow {}^7F_j$ ($j = 1-4$) transitions that differ in multiplicities and relative intensities (Figure 6, Table 6), pointing to different geometries around Eu^{III}. For

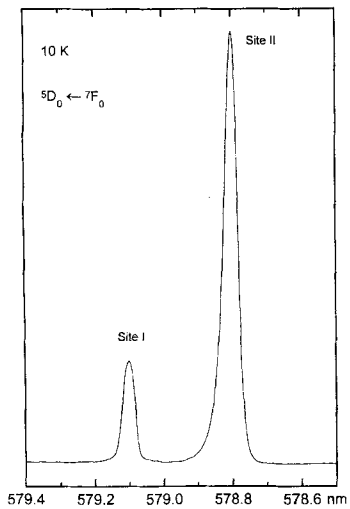

Figure 5. Excitation spectrum of $[Eu(L^5)_2(TfO)_2(OH_2)]TfO$ (**1**) in the range of the $^5D_0 \leftarrow {}^7F_0$ transitions at 10 K (λ_{an} = 590.2 nm).

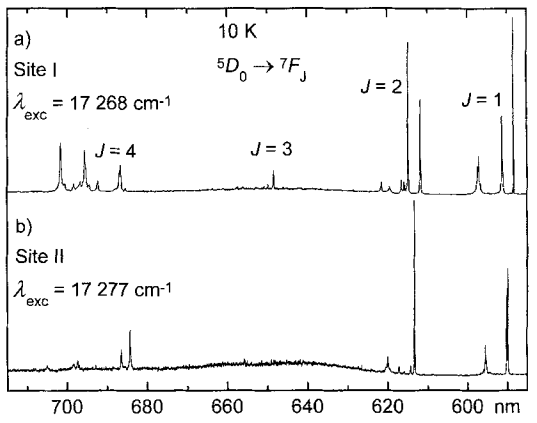

Figure 6. Part of the laser-excited emission spectrum of $[Eu(L^5)_2(TfO)_2(OH_2)]TfO$ (**1**) at 10 K upon selective excitation at a) $\lambda_{exc} = 17268$ cm^{-1} (site I) and b) $\lambda_{exc} = 17277$ cm^{-1} (site II).

site I, the local symmetry is low as shown by 1) the three regularly spaced components of the $^5D_0 \rightarrow {}^7F_1$ transition and 2) the five and nine components observed for $^5D_0 \rightarrow {}^7F_2$ and $^5D_0 \rightarrow {}^7F_4$, respectively (Table 6), which correspond to the maximum multiplicity ($2J+1$).[30] This emission spectrum is compatible with the nonacoordinate Eu^{III} site found in the crystal structure of $[Eu(L^5)_2(TfO)_2(H_2O)]^+$. The $Eu(^5D_0)$ lifetime of site I (0.61 ± 0.03 ms at 10 K) is short compared to that found for nonacoordinate Eu^{III} in $[Eu(L^2)_3]^{3+}$, where no water molecule is bound to the metal (1.83 ms). An estimation based on the relationship given in Equation (1)[31] with $A_{Eu} = 1.05$ and, as an

$$q = A_{Eu}(\tau_{H_2O}^{-1} - \tau_{D_2O}^{-1}) \quad (1)$$

0947-6539/97/0310-1664 $ 17.50+.50/0 Chem. Eur. J. 1997, 3, No. 10

Table 6. Corrected integrated intensities (I_{rel}) and main identified Eu(^7F_J) energy levels (cm^{-1}, $J = 1-4$, origin $^7F_0$) for sites I and II in $[Eu(\mathbf{L^5})_2(TfO)_2(OH_2)]TfO$ (**1**) as calculated from luminescence spectra at 10 K (λ_{exc}: $^5D_0 \leftarrow {}^7F_0$).

Level	Site I	I_{rel}	Site II	I_{rel}
$^7F_0$ (λ_{exc}) [a]	17268		17277	
$^7F_1$	273	1.00	325	1.00
	357		333	
	526		486	
$^7F_2$	924	0.85	973	1.00
	1008		1001	
	1035		1148	
	1118			
	1179			
$^7F_3$	1848	0.09	–	[b]
$^7F_4$	2707	1.35	2662	0.84
	2712		2711	
	2827		2941	
	2869		2959	
	2894		3093	
	2919			
	2949			
	2998			
	3016			

[a] Energy of the $^5D_0 \leftarrow {}^7F_0$ transition (cm^{-1}) used as λ_{exc} for the laser-excited emission spectra. [b] Too weak to measure.

approximation, $\tau_{D_2O} = 1.83$ ms, yields $q = 1$ for site I as expected from the crystal structure of **1**.

The Eu($^5D_0$) lifetime of site II (0.46 ± 0.01 ms at 10 K) is shorter; this can be rationalized by the coordination of two water molecules to Eu^{III} ($q = 2$ yields $\tau = 0.41$ ms in Equation (1)). The emission spectrum of site II reflects a symmetry higher than that of site I and may be analyzed in terms of an approximate tetragonal symmetry. For instance, there are only two main transitions to the $^7F_1$ level $A \rightarrow A$ and $A \rightarrow E$, with the latter further split into two closely spaced components ($8\ cm^{-1}$) as a result of a slight deviation from the idealized symmetry or distortions induced by the excitation to the $^5D_0$ level.[6] The transitions to the $^7F_4$ level may be interpreted as $A \rightarrow A$ and $2 \times A \rightarrow E$, where the latter transitions are further broken up into two components separated by 49 and 18 cm^{-1}, respectively. Transitions to the $^7F_2$ level display one intense band and two to three weaker ones, and are more difficult to interpret precisely (Figure 6). From these data, we conclude that Eu^{III} is decacoordinated in site II by two meridionally tridentate ligands $\mathbf{L^5}$, two monodentate triflate anions, and two water molecule in a pseudo-bicapped inverted square-antiprism arrangement (Figure 7),[32] as previously reported for a related 1:2 complex

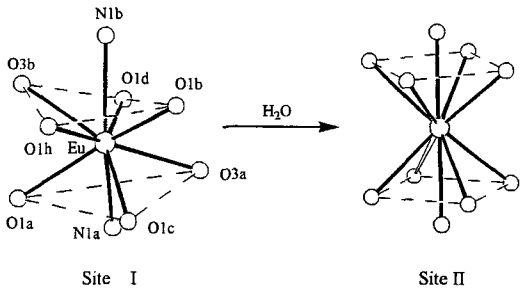

Figure 7. Schematic representation of sites I and II (approximately D_4) in **1** as found by emission spectroscopy. The pseudo-rectangular faces of the tetragonal antiprism are shown with dashed lines.

$[Eu(2,6\text{-bis(benzimidazol-2'-yl)pyridine})_2(NO_3)_2]^+$.[33] We suspect that site II results from the partial hydration of site I, which occurs during the separation of the crystals of **1** from the mother liquor (Figure 7).

The nephelauxetic parameter ($\delta_{O-ester}$) associated with ester groups bound to Eu^{III} has been estimated using the empirical Equation (2) of Frey and Horrocks.[34] For nonacoordinate

$$\tilde{\nu} = \tilde{\nu}_0 + C_{CN} \sum_i n_i \delta_i \qquad (2)$$

Eu^{III} in site I, the energy of the $^5D_0 \leftarrow {}^7F_0$ transition at 295 K is $\tilde{\nu} = 17280\ cm^{-1}$ (correction of $1\ cm^{-1}/24$ K),[30] and the use of $\tilde{\nu}_0 = 17374\ cm^{-1}$,[34] $C_{CN} = 1$,[34] $\delta_{N-heterocyclic} = -15.3$,[7,13] $\delta_{O-water} = -10.4$,[34] and $\delta_{O-triflate} \approx \delta_{O-nitrate} = -13.3$ [34] leads to $\delta_{O-ester} \approx -6.6$. This small nephelauxetic parameter[34] is consistent with a weak interaction between the O donor atom of ester groups and Eu^{III}.

Quantum yields of $[Ln(\mathbf{L^5})_3]^{3+}$ (Ln = Eu, Tb) in acetonitrile: Solutions of $[Ln(\mathbf{L^5})_3]^{3+}$ were prepared in situ in anhydrous acetonitrile at concentrations of 10^{-3} M. Although lower concentrations (10^{-4}–10^{-6} M)[29] are commonly used to minimize self-quenching processes, dissociation of $[Ln(\mathbf{L^5})_3]^{3+}$ becomes problematic at low concentration, and a 10^{-3} M solution represents a reasonable compromise between self-quenching and decomplexation. According to the stability constants of Table 3, we calculate that the following species are formed under these conditions: $\mathbf{L^5}$: 16%; $[Eu(\mathbf{L^5})]^{3+}$: 0%; $[Eu(\mathbf{L^5})_2]^{3+}$: 14%; and $[Eu(\mathbf{L^5})_3]^{3+}$: 70%. The measured relative quantum yields and lifetimes of $[Ln(\mathbf{L^5})_3]^{3+}$ are collected in Table 7. In anhydrous acetonitrile, the lifetimes of the Eu($^5D_0$) and Tb($^5D_4$) levels are long; this implies that no OH oscillator interacts with the metal ions, despite the limited thermodynamic and kinetic stability of these complexes. Compared to that of $[Eu(\mathbf{L^2})_3]^{3+}$ in acetonitrile ($\Phi_{rel} = 6.6 \times 10^{-3}$),[4] the quantum yield of $[Eu(\mathbf{L^5})_3]^{3+}$ shows an improvement by a factor 400, which is attributed to a better match between the energies of the ligand-centered and metal-centered excited states involved in the resonant $\mathbf{L^5} \rightarrow Eu^{III}$ energy transfer processes.[35] It has been shown that an inadequate overlap between the emission spectrum of the donor ($\mathbf{L^5}$) and the absorption spectrum of the acceptor (Eu^{III}) prevents efficient energy transfer.[29,30,35] We notice that the broad ligand-centered $^3\pi\pi^*$ level, which is expected to be involved in the $\mathbf{L^5} \rightarrow Eu^{III}$ energy transfer process,[29,30,35] is blue-shifted for coordinated $\mathbf{L^5}$ compared to coordinated $\mathbf{L^2}$, as measured from the emission spectra of Gd^{III} complexes in the solid state (vide supra), and displays a better overlap with Eu($^5L_6$) and Eu($^5D_3$) levels. The quantum yield and Eu($^5D_0$) lifetime of $[Eu(\mathbf{L^5})_3]^{3+}$ are very sensitive to the addition of water; this confirms the limited protection of the metallic site in solution (Table 7). $[Tb(\mathbf{L^5})_3]^{3+}$ is only marginally more luminescent than $[Tb(\mathbf{L^2})_3]^{3+}$ ($\Phi_{rel} = 0.74$).[4] As a result of the higher energy of the $^3\pi\pi^*$ ligand-centered excited states in $\mathbf{L^5}$, a reduced back-transfer Tb($^5D_4$) $\rightarrow {}^3\pi\pi^*$ is expected for $[Tb(\mathbf{L^5})_3]^{3+}$, which could be responsible for the larger quantum yield.[36] As observed for the Eu complex, addition of water severely alters the emission properties of $[Tb(\mathbf{L^5})_3]^{3+}$.

  0947-6539/97/0310-1665 $ 17.50+.50/0

Table 7. Quantum yields (Φ_{rel}) relative to $[Eu(terpy)_3]^{3+}$ and $[Tb(terpy)_3]^{3+}$ (terpy = 2,2′:6′,2″-terpyridine) and lifetimes (τ) of the $Eu(^5D_0)$ and $Tb(^5D_4)$ levels for $[Ln(\mathbf{L^5})_3]^{3+}$ (Ln = Eu, Tb) in anhydrous acetonitrile at 298 K [a].

Compd	Conc. [b]	Added H_2O (M)	λ_{exc} (nm)	ε_{exc} ($M^{-1}cm^{-1}$)	Φ_{rel} [c]	τ (ms)
$[Eu(terpy)_3]^{3+}$	10^{-3}	0	371	549	1.0	–
$[Eu(\mathbf{L^5})_3]^{3+}$	10^{-3}	0	291	328	2.7	1.98(4)
$[Eu(\mathbf{L^5})_3]^{3+}$	10^{-3}	0.5	290	810	0.11	0.20(1)
$[Eu(\mathbf{L^5})_3]^{3+}$	10^{-3}	1.0	289	965	0.048	0.16(1)
$[Tb(terpy)_3]^{3+}$	10^{-3}	0	364	685	1.0	–
$[Tb(\mathbf{L^5})_3]^{3+}$	10^{-3}	0	291	463	1.7	2.50(6)
$[Tb(\mathbf{L^5})_3]^{3+}$	10^{-3}	0.5	290	752	0.34	0.70(2)
$[Tb(\mathbf{L^5})_3]^{3+}$	10^{-3}	1.0	289	978	0.12	0.55(1)

[a] Absolute quantum yields of $[Ln(terpy)_3]^{3+}$ determined using an aerated aqueous solution of $[Ru(bipy)_3]^{2+}$ as standard are 1.3% for Eu and 4.8% for Tb. [b] Quantum yields are determined for 10^{-3} M solution to minimize decomplexation (see text). [c] Relative errors on Φ_{rel} are typically 10–15%.

Conclusions

Our results demonstrate that ester groups bound to the 2,6-positions of the central pyridine ring in $\mathbf{L^5}$ display a significantly reduced affinity for Ln^{III} compared with carboxamide groups in $\mathbf{L^2}$, but evidence for Ln–O(ester) interactions can be obtained both in the solid state and in solution. The tridentate binding unit $\mathbf{L^5}$ produces kinetically labile mononuclear triple-helical lanthanide complexes of low stability, $[Ln(\mathbf{L^5})_3]^{3+}$, which are not suitable for use as building blocks in organized supramolecular devices.[1] The limited protection of the Ln^{III} site in $[Ln(\mathbf{L^5})_3]^{3+}$ severely limits the control of spectroscopic properties, but the increased quantum yield of $[Eu(\mathbf{L^5})_3]^{3+}$, compared to $[Eu(\mathbf{L^2})_3]^{3+}$, is pertinent for the design of efficient sensitizers in triple-helical complexes. Ester groups bound to pyridine rings are thus promising candidates for the fine-tuning of $\mathbf{L} \rightarrow Eu^{III}$ energy transfers, provided that the triple-helical structure is ensured by supplementary stabilizing effects. The use of noncovalent d-block tripods to control and organize the coordination of unsymmetrical tridentate binding units possessing terminal ester groups should lead to stable noncovalent lanthanide podates with improved luminescent properties. The complexes $[Ln(\mathbf{L^i})_3]^{3+}$ ($i = 1,2,5$) thus represent a new library of mononuclear triple-helical lanthanide building blocks with predetermined structural, thermodynamic, kinetic, and spectroscopic properties. The combination of these structural motifs in segmental ligands or podands opens new perspectives for the design of functional polynuclear supramolecular lanthanide devices.

Experimental Section

Solvents and starting materials: See ref. [4].

Preparation of diethyl pyridine-2,6-dicarboxylate ($\mathbf{L^5}$): Pyridine-2,6-dicarbonyl dichloride[41] (612 mg, 3.0 mmol) was poured into dry ethanol (20 mL) and stirred for 30 min. Water (20 mL) and a saturated $NaHCO_3$ solution (40 mL) were added, ethanol distilled under vacuum, and the resulting mixture extracted with CH_2Cl_2 (3 × 200 mL). The combined organic phases were dried (Na_2SO_4) and evaporated to dryness, and the white powder obtained was recrystallized from hexane to give 608 mg of product (0.276 mmol, yield = 92%), m.p. = 42–45 °C. EI-MS: $m/z = 224$ [M^+].

Preparation of $[Ln(\mathbf{L^5})_2(TfO)_2(OH_2)]TfO \cdot n H_2O$ (1: Ln = Eu, $n = 0$; **2**: Ln = Gd, $n = 1$; **3**: Ln = Tb, $n = 0$): $Ln(TfO)_3 \cdot n H_2O$ ($n = 1$–2.2, 0.032 mmol) and $\mathbf{L^5}$ (21.5 mg, 0.097 mmol) were dissolved in THF (3 mL). Over 3 d *tert*-butyl methyl ether was slowly diffused into the solution to give 88–94% yields of the products as white powders after isolation and drying. X-ray quality crystals of $[Eu(\mathbf{L^5})_3(TfO)_2(OH_2)]TfO$ (**1**) were obtained by means of the same procedure, but the prisms were not separated from the mother liquor; if this is removed, the prisms are readily transformed into a microcrystalline powder. Complexes **1–3** were characterized by their IR spectra and gave satisfactory elemental analyses (Table S1 in the Supporting Information).

Preparation of $[Ln(\mathbf{L^5})_3](TfO)_3$ (Ln = La, Ce, Pr, Nd, Sm, Eu, Gd, Tb, Lu, Y): These complexes were prepared in situ for ^1H NMR studies in solution. $Ln(TfO)_3 \cdot n H_2O$ (0.023 mmol; Ln = La, Ce, Pr, Nd, Sm, Eu, Gd, Tb, Lu, Y, $n = 0.5$–2.2) and $\mathbf{L^5}$ (15.7 mg, 0.07 mmol) were dissolved in degassed CD_3CN (0.7 mL) to give a 0.033 M solutions of $[Ln(\mathbf{L^5})_3](TfO)_3$ the purity of which was checked by ^1H NMR spectroscopy. For photophysical studies CH_3CN was used instead of CD_3CN, and the resulting solution was evaporated, and the residual solid dried under vacuum and then diluted to 10^{-3} M with anhydrous CH_3CN.

Crystal structure determination of $[Eu(\mathbf{L^5})_2(TfO)_2(OH_2)]TfO$ (1): Fragile crystal were mounted from the mother liquor on a quartz fiber with perfluoropolyether oil RS3000®.

Crystal data: $EuC_{25}H_{28}N_2O_{18}F_9S_3$, $M_r = 1063.6$, trigonal, $P\bar{3}$, $a = 20.875(2)$, $c = 15.239(2)$ Å, $U = 5751(1)$ Å^3 (by least-squares refinement of 21 reflections, $15 \le 2\theta \le 25°$), $Z = 6$, $\rho_{calcd} = 1.84$ g cm^{-3}, $F(000) = 3168$. Colorless hexagonal prisms. Crystal dimensions $0.12 \times 0.12 \times 0.40$ mm, $\mu(Mo_{K\alpha}) = 1.919$ mm^{-1}.

Data collection and processing: Stoe STADI4 diffractometer, $T = 150$ K, ω–2θ scan, scan width $= 1.05 + 0.35 \tan\theta$, scan speed $0.10° s^{-1}$, $Mo_{K\alpha}$ radiation ($\lambda = 0.7107$ Å); 9708 reflections measured ($3 \le 2\theta \le 48°$; $-24 < h < 24$, $0 < k < 24$, $0 < l < 18$), 6020 unique reflections (R_{int} for equivalent reflections = 0.083) of which 4040 were observable ($|F_o| > 4\sigma(F_o)$). Two reference reflections were measured every 30 min and showed a total variation $< 2.7\sigma(I)$.

Structure analysis and refinement: Data were corrected for Lorentz, polarization and absorption effects[37] ($A^*_{min} = 1.223$, $A^*_{max} = 1.241$). The structure was solved by direct methods using multan 87;[38] all other calculations used XTAL[39] system and ORTEP II[40] programs. Full-matrix least-squares refinements (on F) using weights of $\omega = 1/\sigma^2(F_o)$ gave final values $R = 0.058$, $R_\omega = 0.037$, for 523 variables and 4040 contributing reflections. Two triflates are coordinated to Eu^{III} and three triflates are located about threefold axes (one in special position 2d and two in special position 2c). All non-H atoms were refined with anisotropic displacement parameters. H atoms were placed in calculated positions and contributed to F_c calculations. The final Fourier difference synthesis showed a maximum of +2.23 and a minimum of −2.38 e Å^{-3}.

Crystallographic data (excluding structure factors) for the structure reported in this paper have been deposited with the Cambridge Crystallographic Data Centre as supplementary publication no. CCDC-100258. Copies of the data can be obtained free of charge on application to The Director, CCDC, 12 Union Road, Cambridge CB21EZ, UK (Fax: Int. code +(1223)336-033; e-mail: deposit@chemcrys.cam.ac.uk).

Spectroscopic and analytical measurements: IR, ES-MS, NMR, emission and absorption spectra, as well as spectrophotometric titrations and quantum yield determinations were recorded as described in ref. [4].

Acknowledgments: We gratefully acknowledge V. Foiret and S. Petoud for their assistance in recording the luminescence data. C. P. thanks the Werner Foundation for a fellowship, and J.-C. B. the Fondation Herbette (Lausanne) for a gift of spectroscopic equipment. This work is supported through grants from the Swiss National Science Foundation.

Supporting information is available from the correspondence author. Table S1 lists elemental analyses for complexes **1–3**. Figure F1 shows the non-isostructurality of $[Ln(\mathbf{L^5})_3]^{3+}$ in solution.

Received: March 14, 1997 [F641]

  0947-6539/97/0310-1666 $ 17.50+.50/0

[1] C. Piguet, *Chimia* **1996**, *50*, 144–153.
[2] C. Piguet, J.-C. G. Bünzli, G. Bernardinelli, C. G. Bochet, P. Froidevaux, *J. Chem. Soc. Dalton Trans.* **1995**, 83–97. S. Petoud, J.-C. G. Bünzli, F. Renaud, C. Piguet, *J. Alloys Compd.* **1997**, *249*, 14–24.
[3] S. Petoud, J.-C. G. Bünzli, K. J. Schenk, C. Piguet, *Inorg. Chem.* **1997**, *36*, 1345–1353.
[4] F. Renaud, C. Piguet, G. Bernardinelli, J.-C. G. Bünzli, G. Hopfgartner, *Chem. Eur. J.* **1997**, *3*, 1646–1659.
[5] P. A. Brayshaw, J.-C. G. Bünzli, P. Froidevaux, J. M. Harrowfield, Y. Kim, A. N. Sobolev, *Inorg. Chem.* **1995**, *34*, 2068–2076. J. M. Harrowfield, Y. Kim, B. W. Skelton, A. H. White, *Aust. J. Chem.* **1995**, *48*, 807–823 and references therein.
[6] C. Piguet, A. F. Williams, G. Bernardinelli, J.-C. G. Bünzli, *Inorg. Chem.* **1993**, *32*, 4139–4149.
[7] C. Piguet, J.-C. G. Bünzli, G. Bernardinelli, G. Hopfgartner, S. Petoud and O. Schaad, *J. Am. Chem. Soc.* **1996**, *118*, 6681–6697.
[8] C. Piguet, E. Rivara-Minten, G. Bernardinelli, J.-C. G. Bünzli, G. Hopfgartner, *J. Chem. Soc. Dalton Trans.* **1997** 421–433.
[9] D. M. Rudkevich, W. Verboom, E. van der Tol, C. J. van Staveren, F. M. Kaspersen, J. W. Verhoeven, D. N. Reinhoudt, *J. Chem. Soc. Perkin Trans. 2* **1995**, 131–134. J. Coates, P. G. Sammes, R. M. West, *ibid.* **1996**, 1275–1282. V.-M. Mukkala, M. Helenius, I Hemmilä, J. Kankare, H. Takalo, *Helv. Chim. Acta* **1993**, *76*, 1361–1377.
[10] V. Alexander, *Chem. Rev.* **1995**, *95*, 273–342. M. P. Hogerheide, J. Boersma, G. van Koten, *Coord. Chem. Rev.* **1996**, *155*, 87–126.
[11] J. March, *Advanced Organic Chemistry*, 4th ed., Wiley, New York, **1992**, Chapt. 8, p. 250–252.
[12] N. Sabbatini, A. Casnati, C. Fischer, R. Girardini, M. Guardigli, I. Manet, G. Sarti, R. Ungaro, *Inorg. Chim. Acta* **1996**, *252*, 19–24.
[13] C. Piguet, E. Rivara-Minten, G. Hopfgartner, J.-C. G. Bünzli, *Helv. Chim. Acta* **1995**, *78*, 1541–1566. G. Hopfgartner, C. Piguet and J. D. Henion, *J. Am. Soc. Mass Spectrom.* 1994, **5**, 748–756.
[14] E. Leize, A. Jaffrezic, A. Van Dorsselaer, *J. Mass Spectrom.* **1996**, *31*, 537–544.
[15] G. Wang, R. B. Cole, *J. Am. Soc. Mass Spectrom.* **1996**, *7*, 1050–1058.
[16] G. Hopfgartner, C. Piguet, J. D. Henion, A. F. Williams, *Helv. Chim. Acta*, 1993, **76**, 1759–1766.
[17] E. R. Malinowski, D. G. Howery, *Factor Analysis in Chemistry*, Wiley, New York, **1980**.
[18] J.-C. G. Bünzli, A. E. Merbach, R. M. Nielson, *Inorg. Chim. Acta* **1987**, *139*, 151–152.
[19] R. D. Shannon, *Acta Crystallogr.* **1976**, *A 32*, 751–767.
[20] F. A. Cotton, G. Wilkinson, *Advanced Inorganic Chemistry*, 4th ed., Wiley, New York, **1980**, p. 69–71. V. S. Sharma, J. Schubert, *J. Chem. Educ.* **1969**, *46*, 506–507.
[21] M. Mammen, E. I. Simanek, G. Whitesides, *J. Am. Chem. Soc.* **1996** *118*, 12614–12623
[22] C. Piguet, G. Hopfgartner, B. Bocquet, O. Schaad, A. F. Williams, *J. Am. Chem. Soc.* **1994**, *116*, 9092–9102. D. K. Lavallee, M. D. Baughan, M. P. Phillips, *ibid.* **1977**, *99*, 718–724.
[23] R. Jagannathan, S. Soundararajan, *Indian J. Chem. Sect. A* **1979**, *18A*, 319–321. R. Jagannathan, S. Soundararajan, *J. Coord. Chem.* **1979**, *9*, 31–35.
[24] R. D. Chapman, R. T. Loda, J. P. Riehl, R. W. Schwartz, *Inorg. Chem.* **1984**, *23*, 1652–1657.
[25] A. D. Sherry, C. F. G. C. Geraldes in *Lanthanide Probes in Life, Chemical and Earth Sciences* (Eds.: J.-C. G.Bünzli, G. R. Choppin), Elsevier, Amsterdam, **1989**, Chapt. 4.
[26] D. A. Durham, G. H. Frost, F. A. Hart, *J. Inorg. Nucl. Chem.* **1969** *31*, 833–838.
[27] J.-L. Pascal, M. E. M. Hamidi, *Polyhedron*, **1994**, *13*, 1787–1792.
[28] G. A. Orpen, L. Brammer, F. H. Allen, O. Kennard, D. G. Watson, R. Taylor, *J. Chem. Soc. Dalton Trans.* **1989**, S1–83.
[29] N. Sabbatini, M. Guardigli, J.-M. Lehn, *Coord. Chem. Rev.* **1993**, *123*, 201–228
[30] J.-C. G. Bünzli in *Lanthanide Probes in Life, Chemical and Earth Sciences* (Eds.: J.-C. G.Bünzli, G. R. Choppin), Elsevier, Amsterdam, **1989**, Chapt. 7.
[31] W. de W. Horrocks, D. R. Sudnick, *J. Am. Chem. Soc.* **1979**, *101*, 334–340. W. de W. Horrocks, D. R. Sudnick, *Science* **1979**, *206*, 1194–1196. W. de W. Horrocks, D. R. Sudnick, *Acc. Chem. Res.* **1981**, *14*, 384–392.
[32] M. G. B. Drew, *Coord. Chem. Rev.* **1977**, *24*, 179–225.
[33] S. Wang, Y. Zhu, Y. Cui, L. Wang, Q. Luo, *J. Chem. Soc. Dalton Trans.* **1994**, 2523–2530.
[34] S. T. Frey, W. de W. Horrocks, *Inorg. Chim. Acta* **1995**, *229*, 383–390.
[35] J.-C. G. Bünzli, P. Froidevaux, C. Piguet, *New J. Chem.* **1995**, *19*, 661–668.
[36] C. Piguet, A. F. Williams, G. Bernardinelli, E. Moret, J.-C. G. Bünzli, *Helv. Chim. Acta* 1992, **75**, 1697–1717.
[37] E. Blanc, D. Schwarzenbach, H. D. Flack, *J. Applied Crystallogr.* **1991**, *24*, 1035–1041.
[38] P. Main, S. J. Fiske, S. E. Hull, L. Lessinger, D. Germain, J. P. Declercq, M. M. Woolfson, *MULTAN 87*; Universities of York, England, and Louvain-La-Neuve, Belgium, **1987**.
[39] S. R. Hall, J. M. Stewart, Eds. *XTAL 3.2 User's Manual*; Universities of Western Australia and Maryland, **1992**.
[40] C. K. Johnson, *ORTEP II; Report ORNL-5138*; Oak Ridge National Laboratory, Oak Ridge, Tennessee, **1976**.

  0947-6539/97/0310-1667 $ 17.50+.50/0